

# An assessment of 3D scanning methods in physical models

R. Capitão<sup>a,\*</sup>, R. Lemos<sup>a</sup>, C.J.E.M. Fortes<sup>a</sup> and R. Jónatas<sup>a</sup>

<sup>a</sup> *Hydraulics and Environmental Department, National Laboratory for Civil Engineering (LNEC), Lisboa, Portugal*

\*Corresponding author: Avenida do Brasil 101, 1700-066 Lisboa, Portugal, rcapitao@lneec.pt

**ABSTRACT:** The evaluation of damage progression caused by wave action on physical models of rubble-mound breakwaters can be accomplished through two types of methods: quantifying the movements and falls of the resistant armor elements by visual inspection (the traditional, classical method) or determining the eroded volumes and depths between consecutive surveys of armor layers using sensors and photogrammetric methods (3D scanning methods). Of the latter, one may use techniques such as the so-called "Kinect", "Photogrammetry" and "LiDAR". The end-product of these techniques is, among others, point clouds, which allow obtaining three-dimensional surface models. In this paper, four of the latter techniques (3D scanning methods) are briefly described, and a comparison is made between them regarding their usability in current tests, their advantages and disadvantages, among themselves for a study case of the physical 3D model of the Ericeira breakwater. In evaluating survey quality across the four methods, RMSE (root mean square error) was employed to align obtained point clouds with ground control points (GCP). Notably, Photogrammetry, Kinect, and Azure techniques showed excellent RMSE values. Conversely, the LiDAR-derived-method cloud, using a smartphone with LiDAR sensor and 3dScanner app, fails to yield acceptable and accurate results for the research objectives of this paper.

**KEYWORDS:** *physical modelling, breakwater, damage progression, reconstruction techniques, 3D scans.*

## 1 INTRODUCTION

2 Physical model tests are often used as a  
3 fundamental tool in the design of rubble-mound  
4 breakwaters, which allows the hydraulic behavior  
5 of these structures to be easily studied under given  
6 conditions of wave action. The main purpose of  
7 these tests is to study the stability of the structure,  
8 and to infer on the possible progression of damage  
9 (if any) through the quantification of movements  
10 and falls of the resistant armor layer elements.  
11 Normally, the identification of movements and  
12 falls of these elements is performed by visual  
13 inspection during the test period. However, this  
14 technique has some limitations, among which is  
15 that it is very dependent on the experience of the  
16 observer. Therefore, to better identify, and even  
17 measure those displacements, other  
18 methodologies have been used, such as photo-  
19 grammetry and 3D scans with position sensors.  
20 More recent methods of evaluation of damage  
21 progression caused by wave action on physical  
22 models involve non-intrusive surveys, utilizing  
23 photogrammetric techniques with RGB sensors,  
24 depth sensors based on the Time of Flight (ToF)  
25 methodology, and LiDAR (Light Detection And  
26 Ranging) laser scanning sensors. Depending on  
27 the survey conditions and the post-processing

28 methodology of the acquired point clouds, these  
29 techniques enable the generation of  
30 three-dimensional surface models with varying  
31 degrees of accuracy.  
32 One of the techniques to obtain three-dimensional  
33 surveys of breakwater models is using a  
34 Microsoft® Kinect position sensor, a depth  
35 sensor based on the Time of Flight (ToF) method.  
36 Soares *et al.* (2017) assessed the use of this sensor  
37 to detect movements of perfect cubes and  
38 tetrapods in two-dimensional (2D) physical  
39 models. Musumeci *et al.* (2018) conducted  
40 surveys of the submerged part of the slope of  
41 breakwaters using the Kinect sensor during 2D  
42 testing with Accropode® artificial blocks. Sande  
43 *et al.* (2018) conducted tests aiming at an  
44 approach to the validation of the surveys with the  
45 Kinect sensor, with determination of the variation  
46 of its accuracy depending on the parameters and  
47 distances to the sensor used in the surveys. Lemos  
48 *et al.* (2022) evaluated damage evolution of  
49 rubble-mound breakwaters based on aero  
50 photogrammetric surveys using both Kinect  
51 sensor and photogrammetric techniques.  
52 The Microsoft Azure Kinect is an upgraded  
53 version of the previous, it also incorporates depth,  
54 IR and RGB sensors but of a more refined, more

55 accurate kind. Utilizing the Azure Kinect SDK  
 56 (software development kit), surveys with this  
 57 low-cost equipment involve swift scanning as the  
 58 user moves across the designated area.  
 59 Another technique is based on photogrammetry  
 60 and has been successfully used in several works,  
 61 in various areas, e.g., recently in the area of  
 62 monitoring (Kwasi and Jayson-Quashigah, 2021).  
 63 It uses the Structure-from-Motion (SfM) method  
 64 to calculate camera positions and orientation with  
 65 and without ground control points (GCP) (Pepe  
 66 and Costantino, 2020).  
 67 Finally, one also deemed interesting to consider a  
 68 third low-cost technique, consisting in the use of  
 69 a smartphone with a built-in LiDAR sensor and  
 70 the 3dScanner iOS app to perform 3D scanning of  
 71 the model. At first sight, this methodology seems  
 72 promising, since it presents portability, ease of  
 73 use and cost as great advantages over the other  
 74 techniques.  
 75 Any of these methods can produce point clouds,  
 76 used to obtain surface models, profile extraction  
 77 and eroded volume calculations. However, the  
 78 accuracy of the results obtained and the ease of  
 79 use in a laboratory environment depends on each  
 80 technique. It is therefore especially important to  
 81 evaluate the performance of the different  
 82 techniques and to identify their main advantages  
 83 and disadvantages.  
 84 In this sense, four techniques of envelope survey  
 85 were evaluated on a 3D physical model of the  
 86 Ericeira breakwater, Portugal, within the scope of  
 87 the three-dimensional physical model tests of this  
 88 structure currently being carried out at the  
 89 National Laboratory for Civil Engineering  
 90 (LNEC).  
 91 The four techniques are entitled “Kinect”,  
 92 “Azure”, “Photogrammetry” and “LiDAR” and  
 93 the study aims to evaluate the best technique to  
 94 obtain three-dimensional surface models to  
 95 ultimately identify changes in the physical model.  
 96 In the following sections, besides describing the  
 97 physical model considered, the above four  
 98 techniques, and the procedures for their use, are  
 99 briefly described, as well as the respective results  
 100 are obtained. A comparison is made between  
 101 them regarding their usability in tests and their  
 102 advantages and disadvantages, among  
 103 themselves.

104 **2 THE PHYSICAL MODEL**

105 The 3D physical model of the Ericeira breakwater  
 106 was built at the experimental facilities of the  
 107 Department of Hydraulics and Environment

108 (DHA) of LNEC, in the TO11 wave tank of the  
 109 Maritime Hydraulics Hall, with dimensions 46.6  
 110 m x 20.6 m. This tank is equipped with 2 mobile  
 111 irregular wave makers of 6.0 m length each, for  
 112 water depths up to 0.75 m (Fig. 1).



Figure 1. Model at LNEC’s experimental facilities.

113  
 114 The model was built and operated according to  
 115 Froude's law of similarity with a geometrical  
 116 scale of 1:75. The tested section is a  
 117 rubble-mound breakwater, with a trapezoidal core  
 118 covered by a filter composed of two rock layers.  
 119 The armor layer at this cross-section is made of  
 120 tetrapods weighing 300 kN, between  
 121 +10.2 m (CD) and -4.5 m (CD), with a porosity of  
 122 around 40%, developing in a 2:3 slope. The head  
 123 contains 550 kN Antifer cubes, regularly placed,  
 124 developing in a 1:2 slope.  
 125 Cross-sections of the trunk and head, at prototype  
 126 scale, are shown in Fig. 2, respectively in the top  
 127 and bottom parts of it.

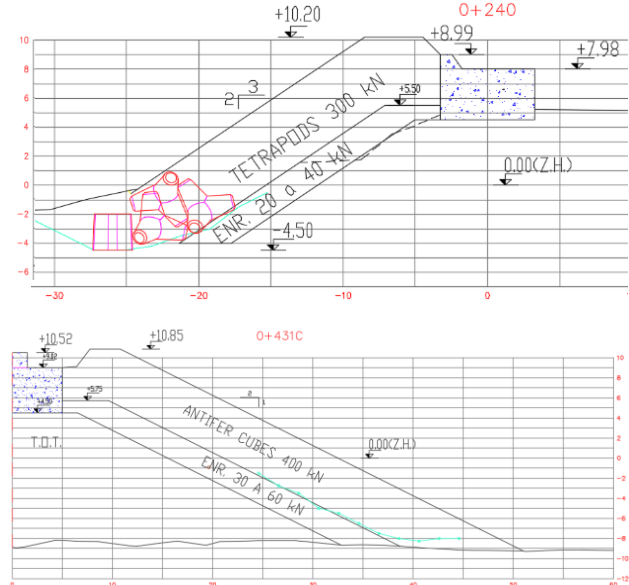


Figure 2. Cross-sections characteristics of breakwater’s trunk (top) and head (bottom).

128 3 TECHNIQUES USED

129 3.1 Introduction

130 For the characterization of undamaged model  
131 (before any tests) the following procedures were  
132 performed:

- 133 • Visual inspection, by accounting the number  
134 of displaced armor units;
- 135 • Three-dimensional survey of the breakwater  
136 model envelope using the Kinect position  
137 sensor and the Kinect Azure sensors.

138 Further, the other two techniques for surveying  
139 the model envelope, using photographs, were also  
140 used. For this, the camera of a smartphone (Apple  
141 iPhone 14 Pro), with 12-M-pixel resolution, was  
142 used. This capture allowed obtaining oblique  
143 photos around the physical model for different  
144 angles and positions.

145 For the 3D reconstruction from these  
146 photographs, two software packages were used:  
147 the commercial software Metashape (Agisoft,  
148 2021) and the iOS mobile phone application  
149 3dScanner (Laan Labs, 2021). Corresponding  
150 techniques used were close-range  
151 photogrammetry and 3D scanning, both used to  
152 generate point clouds.

153 The four techniques (“Kinect”, “Azure”,  
154 “Photogrammetry” and “LiDAR”) are described  
155 below with more detail. For all of them, the tank  
156 was emptied during the 3D scanning and photo  
157 acquisition periods.

158 3.2 Kinect V2

159 This technique uses Microsoft Kinect 2.0 depth,  
160 infrared (IR) and color (RGB) sensors and  
161 Microsoft Kinect Fusion SDK software. Kinect  
162 2.0 sensors, developed for the Microsoft Xbox  
163 game console, are managed to survey the 3D  
164 model at a constant distance of 2.0 m.  
165 Post-processing is conducted using the Cloud  
166 Compare software.

167 The Kinect motion sensor (model 2.0) allows  
168 distance/depth determination through an infrared  
169 projector and a monochrome CMOS  
170 (complementary metal-oxide semiconductor)  
171 sensor, which work complementarily to "see" the  
172 scene in 3-D, regardless of the amount of light in  
173 the room. The device also contains an RGB  
174 camera, which acquires the three components of  
175 color (red, green and blue). The Kinect sensor  
176 uses 'Time of Flight' technology to estimate the  
177 position of a point relative to the sensor, by  
178 measuring the time it takes for an infrared beam  
179 to travel the distance between the sensor and the  
180 object and back, considering the speed of light.

181 For the acquisition of the point clouds, the  
182 free-to-use software Kinect Fusion (Izadi *et al.*,

183 2011), belonging to the software package built  
184 with Microsoft SDK, was used.

185 Fig. 3 shows the equipment used to perform the  
186 three-dimensional survey of the model and the  
187 Kinect Fusion interface. The Kinect operated,  
188 mounted on a tripod, and the acquisition distance  
189 was about 2 m above the model, having been  
190 connected to a computer during the entire data  
191 acquisition phase.

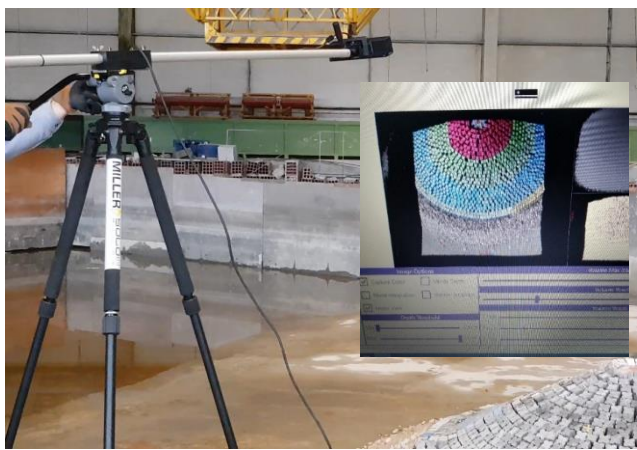


Figure 3. Kinect sensor and Kinect Fusion software interface.

192  
193 Considering the large size of the model and to  
194 obtain the best compromise between the distance  
195 from the sensor to the model and the quality of the  
196 survey, as well as the optimization of the  
197 processing time of the point clouds, the scans  
198 were performed individually, section by section,  
199 keeping the parameters of the sensor used in the  
200 survey constant in all sections. Parameters used in  
201 the survey were: Voxel volume resolution in the  
202 three directions: 512 for the 3 axes; Voxel/m: 256;  
203 acquisition interval: between 0.5 m and 8 m.  
204 Note that the voxel is a 3D unit of the image, just  
205 as for digital photographs, a pixel is a 2D unit of  
206 the image. i.e., it is a volume element that  
207 represents a specific grid value in 3D space. The  
208 obtained point clouds were subsequently merged,  
209 using the open-source free-to-use software  
210 CloudCompare (Girardeau-Montaut, 2006).

211 3.3 Azure Kinect

212 This uses Microsoft Azure Kinect depth, IR and  
213 RGB sensors and experimental software from  
214 GitHub platform. The Microsoft Azure Kinect is  
215 an upgraded version of the previous Kinect 2.0, as  
216 it also incorporates depth, IR and RGB sensors  
217 but of a more refined, more accurate kind.

218 Azure Kinect contains a depth sensor, spatial  
219 microphone array with a video camera, and  
220 orientation sensor as an all in-one small device  
221 with multiple modes, options, and software,  
222 Fig. 4.



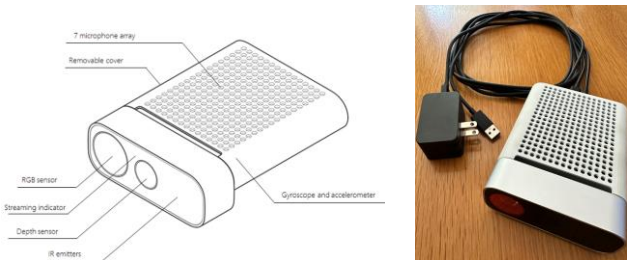


Figure 4. Azure Kinect sensor (Microsoft®).



Figure 6. Azure Kinect acquiring and recording 3D model's data.

Azure Kinect Viewer was also employed to play back the obtained recording (mkv file), by running k4viewer.exe, unfolding the Open Recording tab and opening it, Fig. 7.

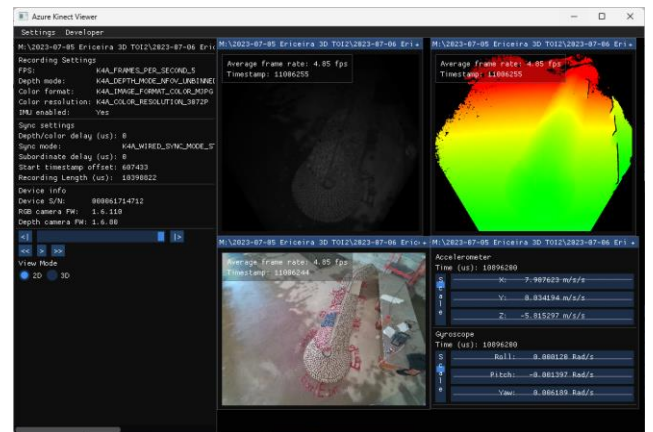


Figure 7. Playing back the Azure Kinect record (2D and 3D).

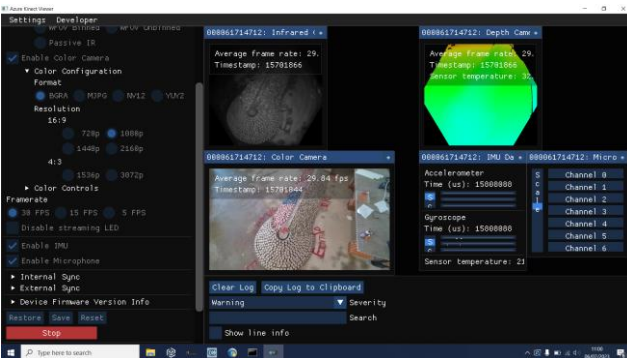


Figure 5. Azure Kinect Viewer interface when viewing the model.

This interface unfortunately does not enable recording of output stream into a file. That must be done separately, which is a problem when one must move the Azure along the model. Therefore, the recording was done by firstly opening a command prompt, providing the path to the Azure Kinect recorder, usually located in the installed tools directory as k4recorder.exe and then recording it to an output.mkv file, Fig. 6.

Two main packages were considered to obtain the point clouds, one Python coded (AK\_FRAEX Azure Kinect Frame Extractor) and a C++ coded (KinectCloud). We used the latter by running "kinectcloud.exe" in windows terminal (or in the Microsoft Visual Studio Enterprise 2022 (64-bit) environment). As a result, one obtained point cloud files e\_1.pts, e\_2.pts..., etc, depending on the selected number of frames. For instance, kinectcloud.exe -e ericeira-All\_10s.mkv created 51-point cloud files (e 1.pts.. e 51.pts) for a 10 sec acquisition with 5 fps, Fig. 8. Loading and concatenating point clouds made use of CloudCompare software.



Figure 8. Point cloud obtained with Azure Kinect mkv.

271  
 272 Fig. 9 and Fig. 10 illustrate this process for the file  
 273 ericeira-All\_10s.mkv. Note that this file was  
 274 obtained using the Azure Kinect about 2 meters  
 275 from the head of the breakwater and over 3 meters  
 276 from the beginning of the trunk, so one expected  
 277 less details on the more distant elements.  
 278 Fig. 9 shows importing and creation of cloud  
 279 points for all frames (at 5 fps) for 10 seconds (51  
 280 in total) of ericeira-Head\_Ext\_10s.mkv file using  
 281 CloudCompare software.

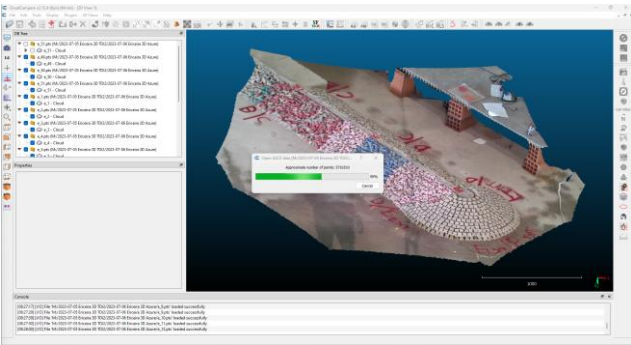


Figure 9. Point cloud import and creation for all frames (5 fps) for 10 seconds (52 in total) of ericeira-Head\_Ext\_10s.mkv file using CloudCompare software.

282  
 283 Fig. 10 shows the merging of all point clouds  
 284 (each obtained for each frame). This was  
 285 accomplished by firstly selecting all the clouds  
 286 and the using command “Merge multiple clouds”.



Figure 10. Point cloud for all frames summed up during 10 sec (at 5 fps).

287 The above process was done for the following  
 288 clouds:

- 289 • ericeira-All\_10s.mkv
- 290 • ericeira-Head\_Ext\_10s.mkv
- 291 • ericeira-Head\_Int\_10s.mkv
- 292 • ericeira-Trunk\_Ext\_10s.mkv
- 293 • ericeira-Trunk\_Int\_1\_10s.mkv
- 294 • ericeira-Trunk\_Int\_2\_10s.mkv

295 Corresponding summed clouds in CloudCompare  
 296 format have the same name with .BIN extension.  
 297 We found, however, that this concatenation is not  
 298 necessary, as is time consuming and does not add  
 299 much information to the obtained point cloud.  
 300 Therefore, we used point clouds for the selected  
 301 static locations, considering just one frame,  
 302 corresponding to the frame before the last one of  
 303 each acquisition, i.e., frame 50.

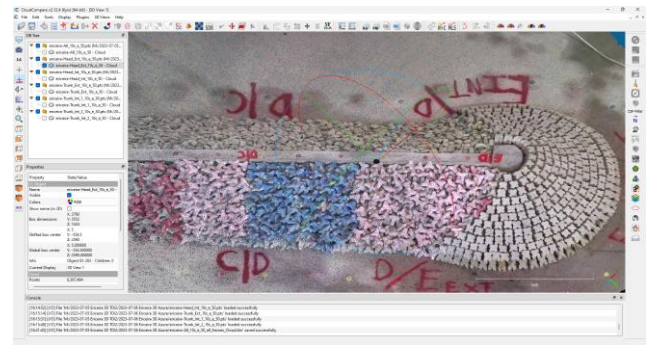


Figure 11. Point cloud creation for frame 50 of ericeira-Head\_Ext\_10s.mkv file using CloudCompare software.

### 304 3.4 Photogrammetry

305 This method uses a photo camera sensor (RGB  
 306 sensor) and photogrammetric software. The  
 307 iPhone 14 Pro smartphone incorporates a rather  
 308 good RGB sensor and therefore it is used here to  
 309 capture oblique photos from various angles and  
 310 positions with significant overlap (+80%) around  
 311 the physical model. The user moves across the  
 312 model's area in both plan and altitude. The  
 313 photogrammetric techniques were applied using  
 314 the commercial (paid) package Agisoft®  
 315 Metashape software. With this software, classical  
 316 photogrammetry tools were applied to a set of  
 317 images with large overlap and obtained from a  
 318 photographic device that moves over the area  
 319 covered by the model, both in plan and altimetry,  
 320 which allowed obtaining orthorectified images,  
 321 orthophoto maps, point clouds and digital terrain  
 322 models (DTM).

323 Fig. 12 illustrates the use of this software, which  
 324 has a very user-friendly interface and allows the  
 325 necessary tasks to be carried out fluidly and  
 326 efficiently.



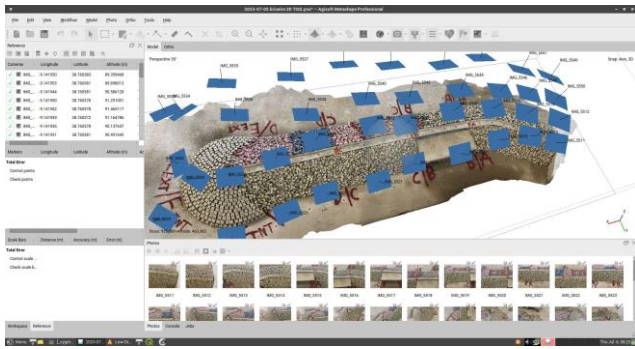


Figure 12. Metashape interface – Photo distribution along the model.

### 3.5 LiDAR

This method uses iPhone 14 Pro's sensors (RGB, ToF and low-cost LiDAR) and the iOS app 3dScanner. This technique uses, through the iOS 3dScanner app, photogrammetric methods on the acquisition, with 3D scanning performed with LiDAR (Light Detection And Ranging) sensor, which is embedded on this simple non-professional smartphone, Fig. 13.

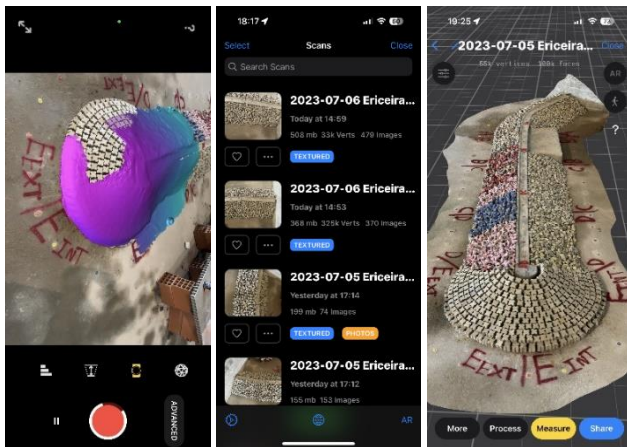


Figure 13. Views of the iOS 3dScanner app interface.

With this technique, the images of the model are obtained by measuring the speed of the light reflected by the elements of the model and consequently obtaining the corresponding distances and other valuable information from the same model. The determination of distances to objects is carried out using a pulsed laser that measures the time difference between the emission of the laser pulse and the detection of the reflected signal, in a similar way to radar technology, which uses radio waves. Since LiDAR technology, in general, is extremely expensive, we thought it would be interesting to use this low-cost LiDAR version incorporated into a simple mobile device to find out about its usefulness in the context of experimentation with physical models. This technique allowed capturing data and create a 3D model while moving the phone across the designated area

covered by the model. The process was eased by using 3dScanner, that also handled processing and exporting functions, although the last were limited since a free version of the app was used.

## 4 COMPARING THE TECHNIQUES

To allow comparison of the described four techniques, a topographic survey of some points of the model was conducted to obtain its coordinates to be used as ground control points (GCP), see Fig. 14.



Figure 14. Control points used for georeferencing the point clouds (in blue) and image capture around the model for Photogrammetry and LiDAR techniques.

These control points were subsequently used to georeference point clouds resulting from each survey technique. The control points (encircled markers in Fig. 14) were located on the model's crown and on the tank floor in the area adjacent to the toe of the slope of the entire model. Their coordinates (x,y,z) were obtained by surveying it with a total station "Leica TCR307". The point clouds alignment using the GPC was performed using the Iterative Closest Point, ICP algorithm (Chen and Medioni, 1991) available in the CloudCompare software. For both the Photogrammetry and LiDAR techniques, photographs were captured using the smartphone camera. For the first technique, one took photographs manually trying to obtain oblique images covering the whole model with overlapping of at least 80%, which resulted in 65 photographs of 12 Mpixel. For the second technique one performed a 3D scanning, which in the end also produced oblique photographs, but of lower resolution, although in an automatic way. According to the image capture algorithm of the application used in this technique (3dScanner App), 429 photographs of ~3 Mpixel were obtained. Tab. 1 shows the characteristics of the equipment and software used and the products generated.

395 Table 1. Characteristics of equipment and software used.

	Kinect	Azure	Photogram- metry	LiDAR
Type	3D scan	3D scan	Photo	3D Scan
Direction	Nadiral	Oblique	Oblique	Oblique
Resolution	-	-	4032 × 3024	1920 × 1440 px2
Number of acquisitions	7 static scans	1 dynamic scan	65 photos	1 scan (429 photos)
Average distance to model	2.0 m	Variable 1-2.0 m	~1.5 m	~1.0 m
Software used for processing	Kinect Fusion	Kinect Cloud	Metashape	3dScanner
Obtained products	Point clouds + DTM + profiles, etc.			

396  
397 The final product of the four techniques is point  
398 clouds, which allow obtaining three-dimensional  
399 surface models and, from these, the extraction of  
400 profiles and the calculation of eroded volumes.  
401 The point clouds obtained with Kinect, Azure and  
402 Photogrammetry were referenced from the  
403 control points, using the Registration tool of  
404 CloudCompare software. Root mean square error  
405 (RMSE) found in the alignment of Kinect and  
406 Photogrammetry point clouds were 0.00971 and  
407 0.01006, respectively.  
408 RMSE translates the average differences found  
409 between the control points used in the cloud  
410 alignment and the same points after the  
411 alignment. Therefore, the error is similar in both  
412 techniques, of the order of 0.01 m, and therefore  
413 very small.  
414 In the case of the LiDAR cloud, obtained with  
415 3dScanner, due to the insufficient resolution of  
416 the cloud (i.e., due to the low density of points of  
417 exported cloud, consequence of using the free  
418 version of 3dScanner), it was not possible to  
419 distinguish the control points located at the base  
420 of the model, being only possible to distinguish  
421 some points of the crest. Therefore, the alignment  
422 was also performed with the Registration tool but,  
423 in that case, homologous points from the cloud  
424 obtained with the Metashape software were used.  
425 Markers at the slope's base and crest were used as  
426 homologous points.

427 5 RESULTS

428 To assess the quality of the surveys obtained with  
429 the four techniques, RMSE (root mean square  
430 error) was determined when aligning the clouds  
431 with the GCP (ground control points).

432 Unfortunately, LiDAR cloud could not be  
433 aligned, as GCP were not visible and therefore  
434 one could not calculate RMSE, which means that  
435 the low-cost LiDAR technique (smartphone with  
436 LiDAR sensor + 3dScanner application) does not  
437 produce acceptable and sufficiently accurate  
438 results for the objective of the present work. In  
439 that way, this technique was disregarded and  
440 omitted here. However, it is important to notice  
441 that this methodology can be used very usefully  
442 as a first indicator of the evolution of damage to  
443 the model during a series of tests. In fact, it is very  
444 quick to use, quite easy to operate and  
445 inexpensive.  
446 On the other hand, the other three techniques  
447 (Kinect, Azure and Photogrammetry) have been  
448 shown to produce particularly good and  
449 comparable results. Tab. 2 shows the RMSE  
450 values obtained for three different clouds, aligned  
451 with the control points, carried out with a total  
452 station.

453 Table 2. Quality assessment of the surveys for three selected  
454 techniques (LiDAR was rejected).

	Kinect	Azure	Photogram- metry
RMSE	0.0048	0.0046	0.0048
N° of points in cloud	3 000 000	2 465 586	5 884 065
N° of GCP	18	13	19

455  
456 For the comparative approach for each point  
457 cloud obtained with those selected techniques, a  
458 surface density analysis was made, by computing  
459 its geometric features with the CloudCompare  
460 software.  
461 Fig. 15, Fig. 16 and Fig. 17 show the point clouds  
462 as well as their surface density maps obtained  
463 with the three techniques considered.

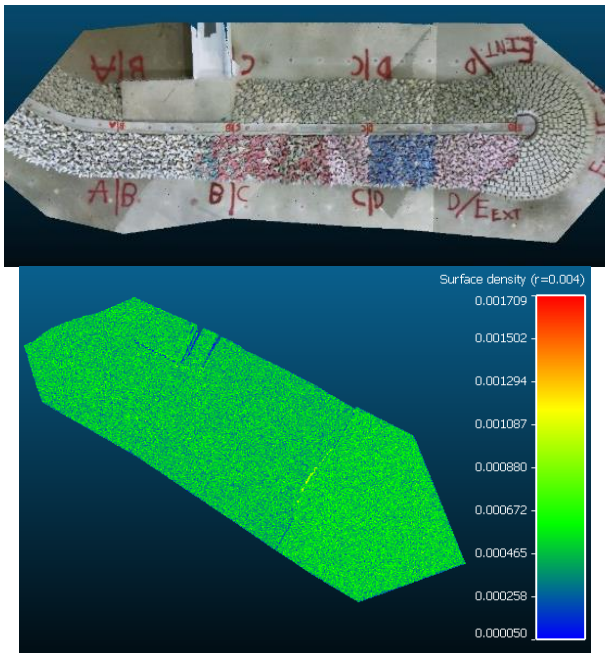


Figure 15. Kinect V2 point cloud and surface density map.



464 The point cloud obtained with the Kinect V2,  
 465 Fig.15, is homogenous, with good quality, despite  
 466 showing some discontinuity due to cloud  
 467 merging.

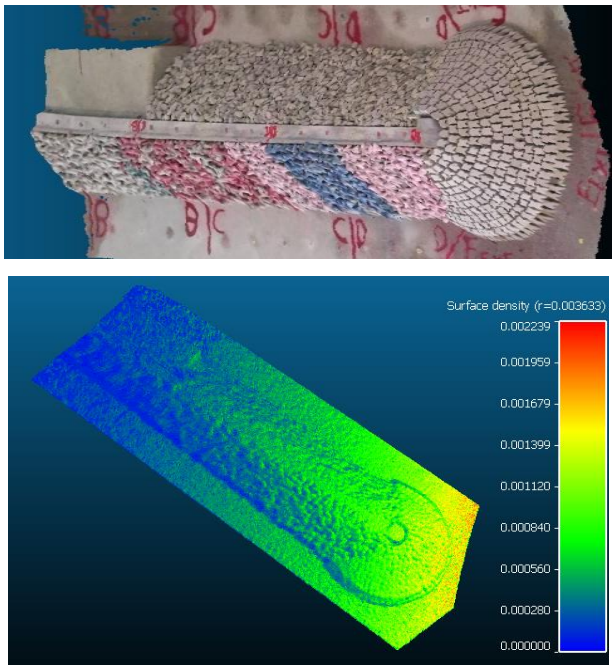


Figure 16. Azure point cloud and surface density map.

468  
 469 The point cloud obtained with the Azure Kinect,  
 470 Fig. 16, is not a uniform point cloud but shows a  
 471 good quality for a cloud obtained from a single  
 472 frame.

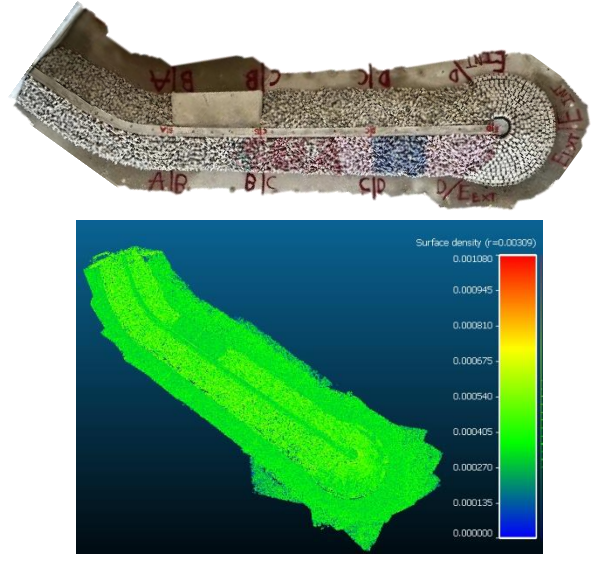


Figure 17. Photogrammetry point cloud and surface density map.

473  
 474 Point cloud obtained with the photogrammetry,  
 475 Fig. 17, exhibits excellent quality, with good  
 476 homogeneity.  
 477 Since this point cloud showed the best quality of  
 478 all, it was considered as a reference to compute  
 479 differences between the remaining clouds.  
 480 Therefore, Fig. 18 and Fig. 19 show the difference  
 481 maps of the trunk and head sections between the  
 482 point cloud obtained by the Photogrammetry

483 technique and the Azure Kinect, and between the  
 484 Photogrammetry technique and Kinect V2  
 485 surveys, respectively.

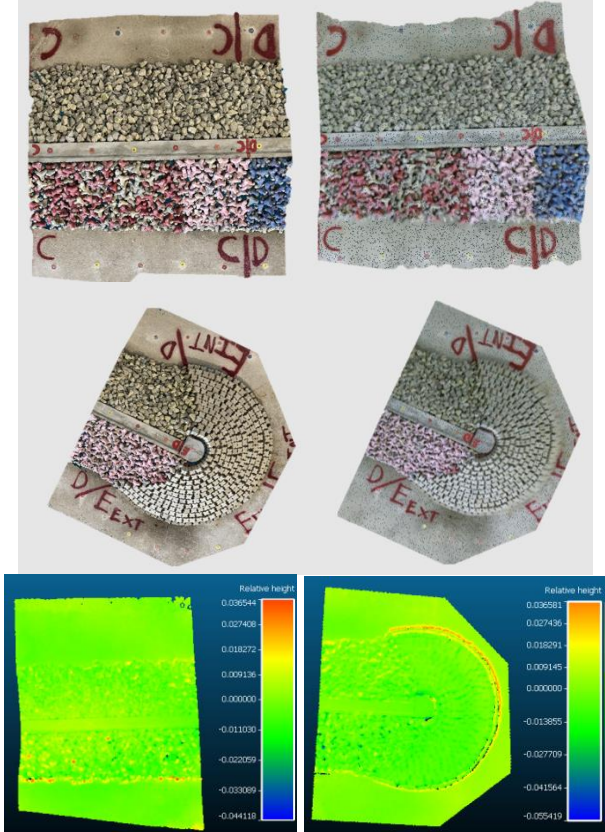


Figure 18. Difference maps between Photogrammetry (left) and Kinect V2 (right) point clouds.

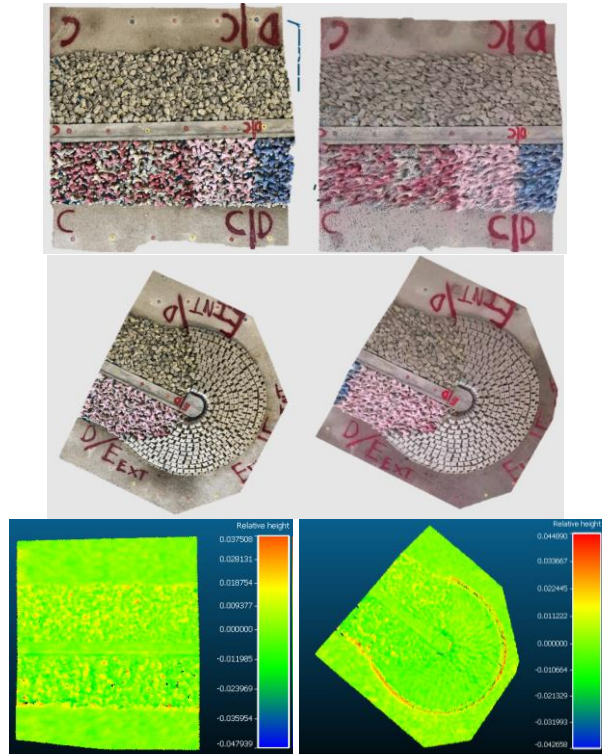


Figure 19. Difference maps between Photogrammetry (left) and Azure Kinect (right) point clouds.

486  
 487 The performance of Kinect v2 and Azure Kinect  
 488 techniques were quite similar, when compared to  
 489 the photogrammetric technique. The altimetric



490 differences were millimetric, except at the toe of  
491 the structure, where the differences found to be  
492 around 0.044 m in the trunk and 0.055 m in the  
493 head zone. These differences are justified by the  
494 decreasing of the accuracy of the point cloud  
495 alignment with the distance to the sensor.  
496 Furthermore, the prismatic shape of the Antifer  
497 cubes at the toe of the head zone contributes to the  
498 error due to the occlusion phenomenon.

## 499 6 CONCLUSIONS

500 Photogrammetry, Kinect and Azure techniques  
501 were found to be quite suitable to evaluate  
502 evolution of damages based on corresponding  
503 point clouds, using RMSE. On the other hand,  
504 cost-effective LiDAR approach used here (a  
505 smartphone and 3Dscanner app) fails to yield  
506 results of acceptable and requisite accuracy for  
507 the current research objectives.

508 The Photogrammetry technique (photogrammetry  
509 with RGB images) was undoubtedly the one that  
510 led to a cloud with the highest number of points,  
511 although it required a lot of post-processing time,  
512 given that it is a photogrammetric method.

513 In the case of the Kinect and Azure techniques  
514 (with depth sensors), point clouds with the same  
515 order of magnitude in terms of number of points  
516 were obtained. The quality of the alignment with  
517 Azure was slightly better, given that a lower RMS  
518 was obtained, using fewer control points.  
519 However, the quality of the RGB obtained with  
520 Azure was much lower than any of the other three  
521 techniques, which made it difficult to select  
522 control points.

523 The Kinect V2 and Azure Kinect techniques thus  
524 produced high-quality results, comparable to  
525 those of the Photogrammetry technique.  
526 However, the latter has the disadvantage of using  
527 a commercial product (Agisoft Metashape),  
528 whose license requires a higher initial investment.  
529 Post-processing the point clouds obtained from  
530 Azure (with motion capture) requires a higher  
531 learning curve for the processing software, as it is  
532 fairly recent. As for the post-processing time of  
533 the clouds obtained with Kinect, this is done in  
534 real time using the Kinect Fusion software used  
535 in the acquisition.

536 However, all the techniques presented here (even  
537 LiDAR) have shown room for improvement  
538 within this work's scope, carrying out surveys  
539 where more time is spent in each zone of the  
540 model, in order to increase the quality of the point  
541 cloud.

## 542 ACKNOWLEDGEMENTS

543 This work was supported by the European Union-  
544 funded projects C2IMPRESS (Horizon Europe,  
545 GA no. 101074004) and LIFE Garachico  
546 (LIFE20 CCA / ES / 001641).

## 547 REFERENCES

- 548 Agisoft (2021). Agisoft Metashape User Manual:  
549 Professional Edition, Version 1.7. Agisoft LLC.  
550 [https://www.agisoft.com/pdf/Metashape-pro\\_1\\_7\\_en.pdf](https://www.agisoft.com/pdf/Metashape-pro_1_7_en.pdf).  
551 Chen Y. & Medioni G. (1991). "Object modelling by  
552 registration of multiple range images". International  
553 Conference on Robotics and Automation, Sacramento,  
554 California.  
555 Girardeau-Montaut, D. (2006). "Détection de changement  
556 sur des données géométriques tridimensionnelles". PhD  
557 thesis.  
558 Izadi, S.; Kim, D.; Hilliges, O.; Molyneaux, D.; Newcombe,  
559 R.; Kohli, P.; Shotton, J.; Hodges, S.; Freeman, D.;  
560 Davison, A.; Fitzgibbon, A. (2011) - Kinect Fusion: real-  
561 time 3D reconstruction and interaction using a moving  
562 depth camera.  
563 Kwasi, A.; Jayson-Quashigah, P. (2021). Unmanned Aerial  
564 Systems. Theoretical Foundation and Applications.  
565 Advances in Nonlinear Dynamics and Chaos (ANDC).  
566 Chapter 7 - UAV photogrammetry and 3D reconstruction:  
567 application in coastal monitoring 2021, Pages 157-174.  
568 Laan Labs (2021). 3d Scanner App™. LIDAR Scan in 3D.  
569 [https://apps.apple.com/us/app/3d-scanner-  
570 app/id1419913995](https://apps.apple.com/us/app/3d-scanner-app/id1419913995).  
571 Lemos, R. (2021). Procedimentos para pós-processamento  
572 de nuvens de pontos provenientes de levantamentos  
573 aerofotogramétricos com drone. Technical report  
574 BSafe4Sea 01/2021, April (in Portuguese).  
575 Lemos, R., Capitão, R., Fortes, C.J.E.M., Henriques, M.J.,  
576 Ferreira, J.C., Jóia, C. (2022). Damage evolution of rubble-  
577 mound breakwaters based on aero photogrammetric  
578 surveys. In 16th International Conference Littoral22 Book  
579 of Abstracts, pp 86-88, 12-16 September 2022. NOVA  
580 School of Science and Technology | FCT NOVA. ISBN:  
581 978-972-99923-6-0.  
582 Miranda, J.C. et al. (2022): AKFruitData: A dual software  
583 application for Azure Kinect cameras to acquire and extract  
584 informative data in yield tests performed in fruit orchard  
585 environments, Elsevier ScienceDirect SoftwareX 20 (2022)  
586 101231. <https://doi.org/10.1016/j.softx.2022.101231>.  
587 Microsoft (2023). Azure Kinect DK documentation.  
588 <https://learn.microsoft.com/en-us/azure/kinect-dk/>  
589 Musumeci, R.; Moltisanti, D.; Foti, E.; Battiato, S. 3-D  
590 monitoring of rubble-mound breakwater damages.  
591 Measurement 2018, 117, 347–364.  
592 Pepe, M.; Costantino, D. (2020). Techniques, tools,  
593 platforms and algorithms in close range photogrammetry in  
594 building 3D model and 2D representation of objects and  
595 complex architectures. Comp.-Aided Des. Applic., 18 (1)  
596 (2020), pp. 42-65, 10.14733/cadaps.2021.42-65.

597 Sande, J.; Peña, E.; Neves, M.G.; Lemos, R.; Figuero, A.;  
598 Reis, M.T.; Alvarellos, A.; Rabuñal, J. 2018. Application  
599 of scanning techniques for damage analysis in rubble  
600 mound breakwaters. In Proceedings of the of CoastLab  
601 2018—7th International Con-ference on the Application of  
602 Physical Modelling to Costal and Port Engineering and  
603 Science, Santander, Spain, 22–26 May 2018.  
604 Soares, F.; Henriques, M.; Rocha, C. Concrete block  
605 tracking in breakwater models. In Proceedings of the of FIG  
606 Working Week, Helsinki, Finland, 29 May–2 June 2017.